Effect of molecular ordering on spin and charge injection in rubrene

K. V. Raman,[1,*] S. M. Watson,[2] J. H. Shim,[1] J. A. Borchers,[2] J. Chang,[1,3] and J. S. Moodera[1]

[1]*Francis Bitter Magnet Laboratory, MIT, Cambridge, Massachusetts 02139, USA*

[2]*National Institute of Standards and Technology, Gaithersburg, Maryland 20899, USA*

[3]*Center for Spintronics Research, Korea Institute of Science and Technology, Seoul, Korea*

(Received 30 July 2009; revised manuscript received 29 October 2009)

Studies have shown that interfaces play a crucial role for efficient spin injection and transport. Here, we address the complex role of interface in spin and charge injection into organic materials by various interface-sensitive characterization tools. Inelastic tunneling spectroscopy and polarized neutron reflectometry were mainly adopted to explore the interfaces of high mobility organic semiconductor rubrene sandwiched by two ferromagnetic electrodes. The dramatic difference in the reported magnetotransport properties and charge injection characteristics in trilayer magnetic junctions have been attributed to the different growth morphology of rubrene molecules at the interface dictated by the presence or absence of a 0.6 nm alumina seed layer. The magnetic contribution of the top ferromagnetic electrode is also influenced by the morphology of the rubrene layer underneath, directly affecting the spin injection efficiency. This work highlights the importance of interface engineering in the development of organic-based spintronics devices.

Spin transport in π-conjugated organic semiconductors (OSs) is necessarily a vast and complex area that is just beginning to be explored.[1] Recent demonstrations of spin transport in organic materials[2–6] have been promising, giving impetus to explore the potential of OSs in spintronics applications. Although their study can be extremely challenging, it is expected to be rich in knowledge. For instance, unlike inorganic semiconductors, OSs have shown significantly complex charge injection and transport mechanisms. To date, several theories have dealt with the transport phenomena: modeling the strong electron-phonon coupling (polarons) and the structural disorder of the molecules to account for the observed transport characteristics in different organic systems.[7–9] Growth-related structural changes in OS films have also been known to influence the transport properties[10] and, consequently, the spin injection and transport, as observed in this work. Due to the complexity associated with organic systems, appropriate characterization methods need to be implemented to understand the spin transport.

In our recent work, we demonstrated a large tunneling magnetoresistance (TMR) of 6% at room temperature, showing a spin-diffusion length of 13 nm in thin amorphous rubrene films ($C_{42}H_{28}$).[11] The study was performed in the tunnel junction structure for hybrid (rubrene film grown on alumina as tunnel barrier) and rubrene (rubrene film grown without alumina seed layer) barriers. In this work, we address the role of interfaces, their influence on the growth morphology of the OS, and hence on the transport properties by performing interface-sensitive characterization by inelastic tunneling spectroscopy (IETS) and polarized neutron reflectometry (PNR) measurements. Charge and spin transport measurements were extended to thick rubrene barriers (>20 nm) to obtain information on the evolution of the film morphology with thickness in both types of junctions.

Samples for IETS measurements were prepared as a metal-insulator-metal structure with a thin rubrene barrier film to form hybrid junctions (HJs) and rubrene junctions (RJs). The layers were all grown *in situ* using a shadow mask technique[3,11] in a deposition chamber with a base pressure of 6×10^{-8} Torr. In the case of HJs, the bottom electrode and a thin Al layer (0.5 nm) were grown at low temperature (80 K). This was followed by short (6–8 s) oxygen plasma exposure (500 W at 60 mTorr) to form a thin alumina seed layer. The rubrene barrier and the top electrode were then deposited at room temperature to form the junction (200×200 μm^2).

IETS is a powerful tool to analyze the active vibrational modes of molecules within the barrier, in probing their orientation, structural, electronic, and chemical modifications.[12,13] The strong electron-phonon coupling in organic materials makes IETS a highly interface-sensitive characterization tool compared to other spectroscopic methods such as Raman and infrared (IR). Unlike Raman and IR spectroscopy, the wavelength of the probing tool (electrons) in IETS is much smaller. As a result, the selection rules, governing the symmetry of the vibrating dipoles with respect to the probing wavelength, are different in IETS and depend only on the orientation of the molecules as predicted and observed experimentally.[13]

IETS was carried out at 4.2 K using a lock-in technique, with an ac modulation of 5 mV at 495 Hz to improve the signal detection. Figure 1 shows the IETS results ($\frac{d^2I}{dV^2}$ *vs V*) for the HJ and the RJ. All the major peaks in the IETS plot were carefully examined for reproducibility. The computed Raman and IR spectroscopy peaks with relative intensities for single-crystal rubrene by Weinberg-Wolf *et al.*[14] are also shown in Fig. 1. The IETS data were also obtained for control junctions with only Al_2O_3 barrier (no rubrene) to identify the peaks due to rubrene molecules in the barrier. The Al-phonon mode at ~33 mV (Ref. 15) and the Al-O stretching modes at ~107 mV (Ref. 16) are identified. For the HJ, the peak position and the relative intensity of the different active phonon modes are found to match well with the Raman and IR peaks obtained for the free standing rubrene single crystals, showing that the rubrene molecules are *not structurally altered* in the *barrier* of *our junctions*. However, for the RJ, strong low-energy modes with additional trap-assisted reso-
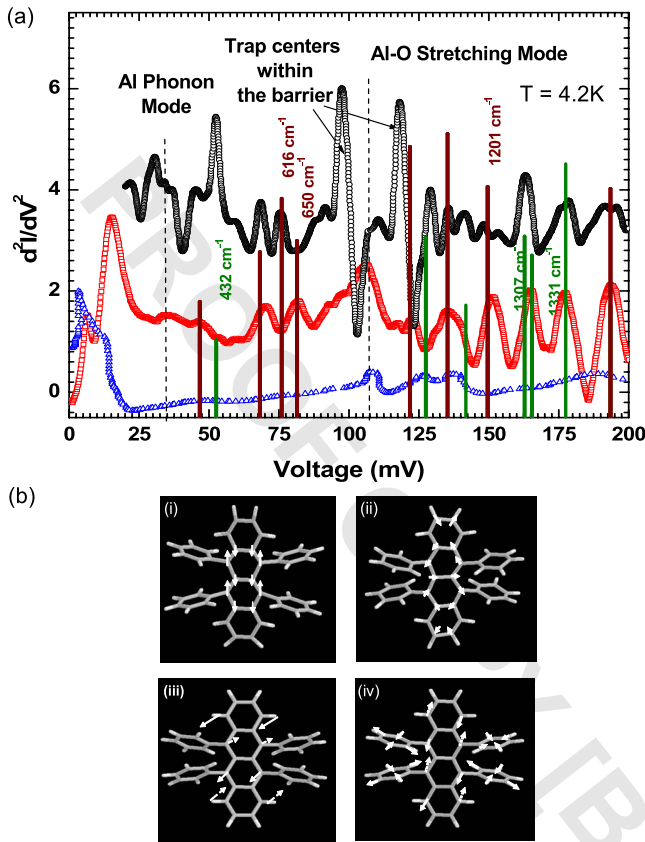
FIG. 1. (Color online) (a) IETS plots of hybrid junctions $[Al(8)/Al_2O_3(0.6)/Rub(6)/Al(10)]$ (black circles) and rubrene junctions $[Al(8)/Rub(10)/Al(10)]$ (red squares) with IETS plot of control junctions $[Al(8)/Al_2O_3(1)/Al(8)]$ (blue triangles) and computed Raman (maroon line) and IR (green line) peaks for single-crystal rubrene included for reference (all thicknesses are in nm). (b) Active molecular vibrational modes observed in hybrid junctions at (i) 1201 cm^{-1} and (ii) 650.1 cm^{-1} (arrows represents vibrations in plane along the tetracene axis) and in rubrene junctions at (iii) 432 cm^{-1} and (iv) 616.4 cm^{-1} (arrows represent vibrations out of plane perpendicular to the tetracene axis). Schematics of the molecular vibration shown here is taken from Ref. 19. The IETS plots are shifted vertically for clarity.

AQ: #2

97 nant states at 100 and 121 mV are observed, suggesting a
98 disordered growth of rubrene films. Based on a previous
99 study on trap-assisted tunneling,[17] the energy level of the
100 trap (V_t) above the electrode Fermi level and the physical
101 position of the trap (d_t) from the bottom electrode are ex-
102 tracted using $V_t=V_rV_f/(V_r+V_f)$ and $d_t=d_oV_f/(V_r+V_f)$, where
103 V_f and V_r are the position of the trap peak in forward and
104 reverse bias, respectively, of the IETS data (reverse bias not
105 shown in the IETS plot for clarity) and d_o is the effective
106 electrical thickness of the barrier. A dielectric constant of 3.0
107 for rubrene was used in estimating d_o.[18] The calculations for
108 the trap states at 100 mV and 121 mV gave a value of V_t
109 =50 mV, d_t=44 Å and V_t=60 mV, d_t=47 Å, respectively.
110 However, the number of trap states and their corresponding
111 location within the barrier were not the same from sample to
112 sample, suggesting extrinsic origin, due to growth-related
113 structural defects.
114   In order to understand the difference in the active vibra-

115 tion modes and their relative intensities observed in the two
116 types of junctions, the IETS data were compared with the
117 molecular vibration simulations reported by Weinberg-Wolf
118 *et al.*[14,19] It is known that in IETS, the tunneling electrons
119 interact preferably with the vibrational modes that involve
120 oscillating bond dipoles parallel to the direction of electron
121 flow.[20–22] In HJ, the peak observed at 81 mV, corresponding
122 to an IR mode (650 cm^{-1}), involves oscillations along the
123 tetracene backbone axis of the rubrene molecule. Similarly,
124 the intense active modes at 150 mV (1201 cm^{-1} IR mode)
125 and 165 mV (1331 cm^{-1} Raman mode) also show vibrations
126 along the tetracene backbone axis [see Fig. 1(b) (i and ii)],
127 strongly suggesting azimuthal (vertically up) growth of ru-
128 brene molecules on the alumina seed layer. In RJ, however,
129 these modes are absent, whereas other modes at 53 mV
130 (432 cm^{-1} Raman mode), 76 mV (616 cm^{-1} IR mode), and
131 163 mV (1307 cm^{-1} Raman mode) are observed, which cor-
132 respond to oscillations transverse to the tetracene backbone
133 axis involving the side rings [see Fig. 1(b) (iii and iv)]. This
134 indicates that in the latter case, the rubrene molecule prefers
135 to grow flat on the electrode resulting in disordered growth
136 of the film. Similar observations of different growth mor-
137 phologies of OSs are reported by other techniques as
138 well[10,23] and may be attributed to the different electronic
139 coupling of the organic molecules with the growth surface
140 controlled by the surface local density of states.[24]
141   Higher-energy modes at 177.5 and 193.5 mV were also
142 seen in both the HJ and RJ, corresponding to the vibrational
143 modes in the side phenyl rings of the rubrene molecule. Few
144 low intensity modes with transverse oscillations are also
145 noted in the HJ at 47 mV (377 cm^{-1} IR mode) and 122 mV
146 (978 cm^{-1} IR or Raman mode), which we interpret as aris-
147 ing from the top rubrene-metal interface. In Fig. 1, the IETS
148 data are shown for junctions with Al electrodes since it was
149 found to give less background noise and help comprehend
150 the information contained in these plots better. With ferro-
151 magnetic (FM) electrodes [Co and Py (or Fe) as the bottom
152 and top electrodes, respectively], a large nonlinear back-
153 ground was present, which smear out the peaks at lower bias
154 ($<\sim70$ mV). However, a systematic and careful study on
155 multiple samples, both with FM and Al electrodes, showed
156 similar activity of the molecular vibrations leading to the
157 same conclusions.
158   Attempts were made to study the evolution of the growth
159 morphology of rubrene with increasing thickness. For thin
160 films (<10 nm), the IETS results concur with the conclu-
161 sions from the cross-sectional transmission electron micro-
162 scope images taken on MTJ structures.[11] It reproducibly
163 showed a considerable dependence of the rubrene film thick-
164 ness on the growth surface: nearly double the barrier thick-
165 ness in HJ compared to RJ, for the same nominal rubrene
166 thickness (2.2 nm read from the *in situ* quartz monitor). For
167 thicker films (>10 nm), IETS looses the sensitivity to dis-
168 tinguish between the interface and bulk molecular layers.
169 This is experimentally observed with the presence of addi-
170 tional second-order peaks in the IETS plot. In such cases, we
171 have tried to study the evolution of the rubrene morphology
172 using thickness measurement and electrical transport mea-
173 surements in an attempt to separately probe the bulk and the
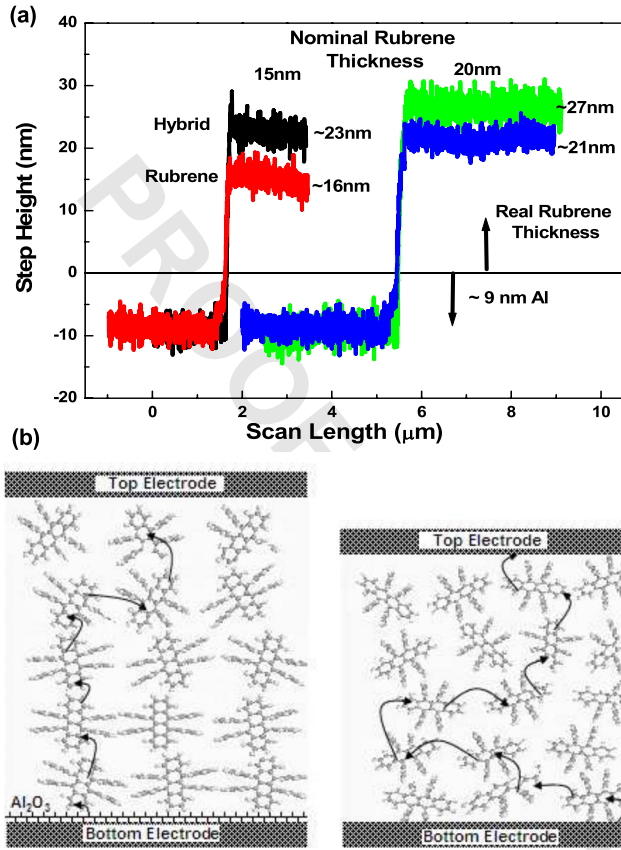174 interface properties. Thickness measurements were per-

AQ #1

FIG. 2. (Color online) (a) Shows the rubrene film thickness measured using P-16 profilometer for Al(6 nm)/Rub(x)/Al(3 nm) and Al(6 nm)/Al$_2$O$_3$(0.7 nm)/Rub(x)/Al(3 nm) with two different values of the nominal thickness: $x=15$ and 20 nm. (b) (Left) Stronger intermolecular electronic coupling in azimuthally grown rubrene films leads to efficient spin injection and enhanced spin transport signals in hybrid junctions. (Right) Disordered nonazimuthal growth in rubrene junction leads to hopping dominant spin injection resulting in spin scattering and weak magnetotransport signals.

175 formed on thick rubrene films grown simultaneously on Al
176 and Al$_2$O$_3$ surfaces with the same nominal thickness (nomi-
177 nal values of 15 and 20 nm), using P16 profilometer, and is
178 shown in Fig. 2(a). A notable difference in the real thickness
179 of the rubrene film for the two types of samples is observed.
180 However, the difference is much less than when the films are
181 thinner.[11] These results well indicate that molecular ordering
182 is an interface effect driven by the underlying seed layer.
183 With increasing thickness, the bulk disorder smears the pref-
184 erential azimuthal growth in HJs. Nevertheless, as we will
185 show next, we do observe some remanence of the interface
186 ordering, which affects the transport even at 20-nm-film
187 thickness. Figure 2(b) schematically shows a model for the
188 rubrene layer growth and its effects on the transport proper-
189 ties.
190   Conductance versus temperature measurements $[G(T)]$
191 were performed for thicker rubrene films and fitted well with
192 existing transport models,[9,25] providing information about
193 the electronic coupling (and hence molecular ordering), both
194 at the injection interface and within the bulk. Figure 3 shows

195 $G(T)$ for the HJ and the RJ at different applied electric field
196 (F) for the nominal rubrene film thickness of 20 nm. It
197 should be noted that the rubrene films were grown simulta-
198 neously for HJ and RJ to avoid any growth-related variation
199 for the two cases. The charge injection model developed by
200 Arkhipov *et al.*[9] was used to analyze the results. Here, the
201 injected current is found by considering injection into the
202 Gaussian distribution of states (with variance σ) in the OS
203 followed by either the return of the carrier to the electrode or
204 its diffusive escape into the bulk. The injected current I_{inj} is
205 therefore found as a product of the tunneling probability
206 $\exp(-2\gamma_i x_o)$ (i.e., the probability of the carrier reaching the
207 position x_0 in the first jump) and the escape probability
208 $w_{\text{esc}}(x_0)$ (Ref. 9)

$$I_{inj} \propto \int_a^\infty dx_o \, \exp(-2\gamma_i x_o) w_{\text{esc}}(x_o)$$ 209

$$\times \int_{-\infty}^\infty dE \, \text{Bol}(E) g[U(x_o) - E],$$ 210

211 where $x=a(\sim 0.6$ nm) is chosen as the surface of organic
212 film, γ_i is the interface related inverse localization radius and
213 $\text{Bol}(E)$ is the Boltzmann factor

$$\text{Bol}(E) = \begin{cases} \exp(-E/k_B T), & E > 0 \\ 1, & E > 0, \end{cases}$$ 214

k_B is the Boltzmann constant 215

216 and $U(x)$ is the energy barrier for injection given by $U(x)$
217 $= \phi - \frac{q^2}{16\pi\varepsilon_o\varepsilon_r x} - qFx$, where ϕ is the energy difference between
218 the Fermi level of the electrode and the highest occupied
219 molecular-orbital level of rubrene, q is the electronic charge,
220 $\varepsilon_o\varepsilon_r$ is the dielectric constant arising due to image forces,
221 and F is the applied electric field. It should be noted that the
222 inverse localization length (γ) contains information about the
223 electronic coupling that can provide structure-related infor-
224 mation. Furthermore, they can have different values at the
225 interfaces (γ_i) and within the bulk (γ_b).
226   The injection model fits our experimental curves in the
227 two junctions with the extracted parameters (ϕ, σ, γ_i) shown
228 in Fig. 3. For the optimized fitting parameters, the model
229 reproducibly matches the experimental curve for different F,
230 supporting the validity of the fits. A large ϕ for RJ (1.03 eV)
231 is inferred compared to HJ (0.49 eV), in agreement with
232 previous studies of thin rubrene barrier tunnel junctions.[11] In
233 addition $\gamma_i^r/\gamma_i^h \sim 10$ (r and h denote RJs and HJs, respec-
234 tively) suggests the anisotropic tunneling injection efficien-
235 cies in the two junctions: better tunneling injection in HJs
236 compared to that in RJs. This may be due to the presence of
237 the alumina tunnel barrier and also due to the azimuthal
238 growth of the rubrene molecules at the interface leading to a
239 better electronic overlap of the rubrene π-electron cloud with
240 the metal. Such effects can be expected to influence spin
241 injection and transport. In our earlier work, related differ-
242 ences were observed in terms of the spin-polarized tunneling
243 and TMR signals.[11]
244   The injection model begins to deviate at low T and low F.
245 Bulk transport,[25] viz., one-dimensional (1D) hopping
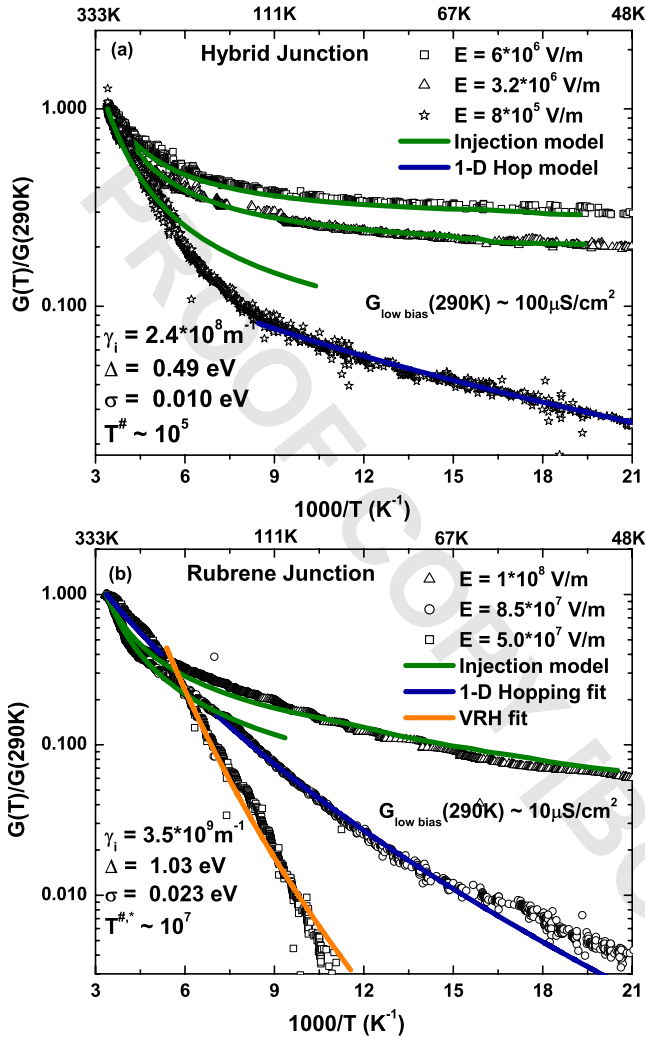
RAMAN *et al.*

FIG. 3. (Color online) Normalized conductance (log scale) vs $1/T$ plotted for (a) hybrid-Co(8)/Al$_2$O$_3$(0.6)/Rub(40)/Fe(8) and (b) rubrene Co(8)/Rub(40)/Fe(8) junctions (thicknesses in nm). The charge injection model is fitted to the experimental curves with the extracted parameters shown. Better fits are obtained from bulk transport models for smaller F at low T.

246 $\{G(T)\alpha\exp[-(T^\#/T)^{-1/2}]\}$ and variable range hopping (VRH)
247 $\{G(T)\alpha\exp[-(T^*/T)^{-1/4}]\}$, where $T^{\#,*}\alpha\gamma_b$ (bulk-related in-
248 verse localization radius), were instead fitted under these
249 conditions, showing a gradual change from charge injection
250 to the bulk transport-limited regime. At such low bias and
251 temperature, a constant density of states near the Fermi level
252 in the organic film is assumed to contribute to bulk conduc-
253 tion. A change from 1D hopping to VRH hopping was ob-
254 served in RJ at lower F. In contrast, no sign of such strong
255 temperature dependence of G was noted in HJ. Only at low
256 electric fields ($F < \sim 1 \times 10^6$ V/m) and low temperatures
257 was the 1D hopping model found to fit the curve for HJ. The
258 fit is shown for the lowest measurable value of F (8
259 $\times 10^5$ V/m). The relatively stronger temperature depen-
260 dence of G observed in RJ compared to HJ suggests the
261 highly disordered growth of rubrene molecules (or weaker
262 electronic coupling) in our RJs. This is supported by the
263 inequality $\gamma_b^r > \gamma_b^h(T^{\#,*}\alpha\gamma_b)$ obtained from the parameters

264 $T^{\#,*}$, extracted using bulk models, signifying stronger inter-
265 molecular coupling in HJs. These results clearly show that
266 the bottom seed layer (Al$_2$O$_3$ in our case) plays an important
267 role for efficient spin injection by influencing the growth of
268 rubrene molecules at the interface. Further, the results sug-
269 gest some remanence of this ordering into the bulk (up to 20
270 nm in this case), providing efficient spin transport.
271   The interface magnetization was probed by PNR mea-
272 surements using the NG1 reflectometer at NIST. Large area
273 samples (~ 1.1 cm^2) with a structure similar to the junctions
274 used for transport studies, with Co and Fe/CoO as the bottom
275 and top layers, were prepared on unetched Si substrates. The
276 nominal thickness of the rubrene film was 10 nm and 20 nm
277 for the hybrid and the rubrene samples, respectively. The
278 samples were cooled down in a magnetic field of 0.7 T to
279 achieve exchange pinning of the Fe layer at the Fe/CoO in-
280 terface. Using a supermirror polarizer and analyzer, the neu-
281 tron beam was polarized parallel to the magnetic field, which
282 was applied in the sample plane, as described in Ref. 26. The
283 reflectivity data were corrected for beam footprint, instru-
284 ment background, and efficiencies of the polarizing elements
285 (typically $>97\%$). Four reflectivity cross sections were mea-
286 sured: R^{++} and R^{--} labeled nonspin flip (NSF) as the neu-
287 tron retains its original polarization after scattering from the
288 sample, and R^{+-} and R^{-+}, labeled spin flip (SF), where the
289 neutron spin flips it polarization, from the up (+) to down
290 state (−) and vice versa, upon scattering. The nuclear scat-
291 tering length density (SLD) of a material or chemical SLD
292 (ρ_{chem}) can be determined from fits to the NSF reflectivity
293 data[26–28] in order to extract a profile of the chemical compo-
294 sition of the film as a function of depth. In addition, the
295 vector magnetization of the film as a function of depth can be
296 ascertained from simultaneous fits to the NSF and SF cross
297 sections. Specifically, the splitting between the NSF reflec-
298 tivity cross sections is sensitive to the component of the
299 magnetization parallel to the applied field. The SF reflectiv-
300 ity is entirely of magnetic origin and is sensitive only to the
301 component of the magnetization perpendicular to the applied
302 field. The NSF PNR data were fit[29] with the REFLPAK (Ref.
303 30) and GAREFL (Ref. 31) software suites to obtain the
304 chemical and magnetic depth profiles. While spin-flip scat-
305 tering was measured at all fields considered in this study, the
306 scattering was observed to be negligible (data not shown),
307 indicating no significant moment perpendicular to the ap-
308 plied field.
309   The reflectivity data collected at 5 K confirmed expecta-
310 tions from SQUID magnetometry that the two FM layer
311 magnetizations are aligned parallel (P) in high fields (H_a
312 $=0.7$ T) and antiparallel (AP) in low fields ($H_a=10$ mT).
313 Figure 4 shows the NSF reflectivity measurement ($R++$ and
314 $R--$) for both the rubrene and the hybrid sample at H_a
315 $=0.7$ T, along with the corresponding depth profile of the
316 nuclear SLD and the layer magnetic moment for the two
317 samples obtained from the fit to the reflectivity data. The
318 most significant difference between the samples includes a
319 lower value of the rubrene nuclear SLD and a larger value of
320 the rubrene layer thickness (~ 1.5 times the nominal thick-
321 ness) obtained for the hybrid sample relative to the rubrene
322 sample (Fig. 4). This result can be explained by the different
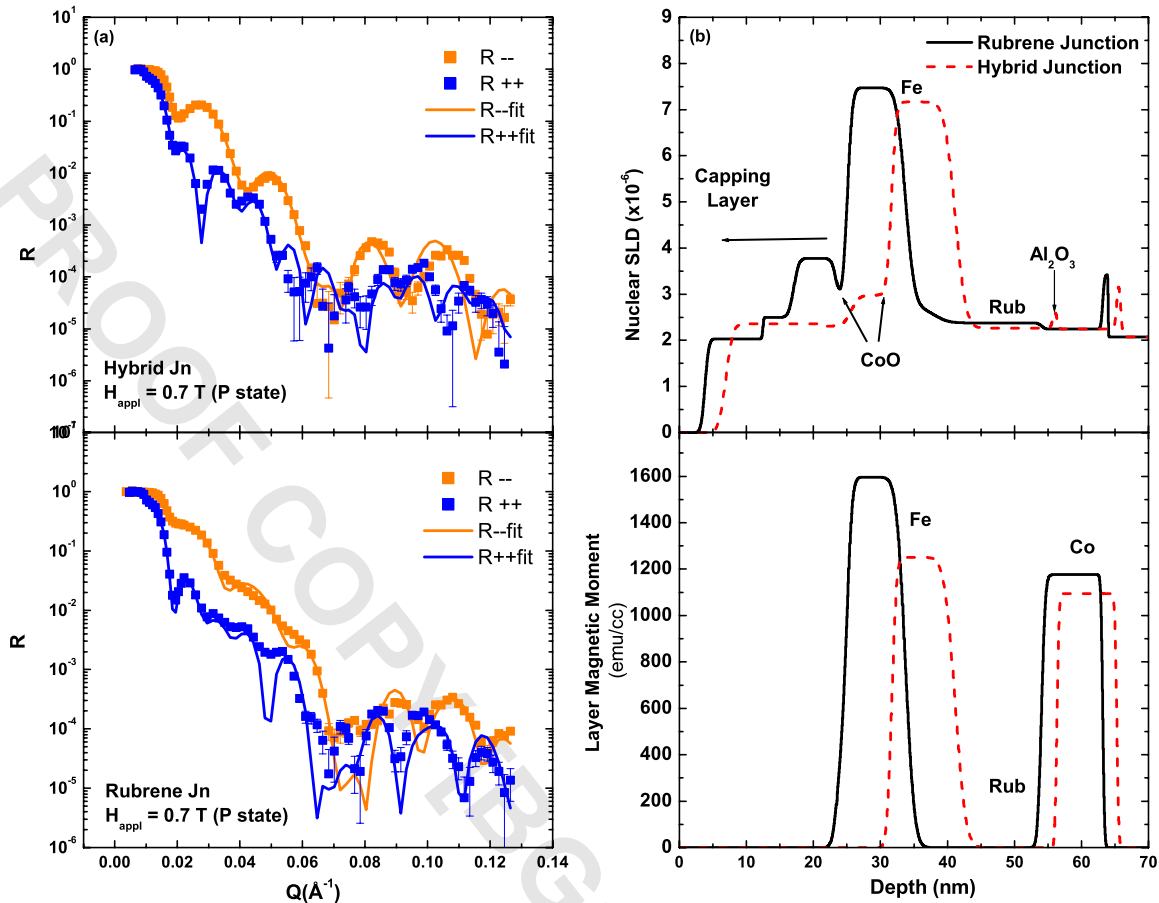323 morphology and packing density of the rubrene molecules

FIG. 4. (Color online) (a) Measured NSF reflectivity data ($R++$ and $R--$) and the corresponding fits for both the rubrene and hybrid samples at H_a=0.7 T. (b) Depth profile of the nuclear SLD (top) and the layer magnetic moment (bottom) obtained from the PNR fits for the hybrid: Si/SiO(1)/Co(8)/Al$_2$O$_3$(0.6)/Rub(15)/Fe(8)/CoO(1.5) and rubrene: Si/SiO(1)/Co(8)/Rub(20)/Fe(8)/CoO(1.5) samples.

324 (Fig. 2) grown on different seed layers (i.e., Co or Al$_2$O$_3$), as
325 described earlier. It is important to note, however, that the
326 structural characteristics of the underlying Co layer in both
327 samples, as determined from PNR, are similar. Specifically,
328 the structural roughness (i.e., corresponding to the width of
329 the interface between the Co layer and the layer above) at the
330 Co/rubrene and Co/Al$_2$O$_3$ interfaces in rubrene and hybrid
331 samples, respectively, is comparable in both samples (Fig. 4).
332 Similar magnetic moments ($\sim$1100 emu/cc) for the free
333 bottom Co layer were also observed in the P and AP states of
334 the hybrid and the rubrene sample. We thus conclude that
335 there is minimal in-plane magnetic domain formation in the
336 bottom FM electrode in the P and AP states because the
337 structural disorder within the Co layer is limited.
338   In general, the moments for all the FM layers in both
339 samples were found to be lower than the bulk values (Co-
340 1422 emu/cc and Fe-1700 emu/cc), which is consistent with
341 expectations for fine-grained polycrystalline thin FM layers
342 and more so for the top FM layers with additional interfacial
343 disorder. The average magnetic moment of the top Fe layer
344 in the hybrid sample is considerably lower, by $\sim$20% for
345 both the AP and P states, compared to the average Fe mo-
346 ment in the rubrene sample (Fig. 4). This difference although
347 puzzling is an interesting result and requires careful interpre-
348 tation within the context of the corresponding structural mor-

349 phology of the upper layers in the two samples. First, it is
350 unlikely that oxidation of the Fe is the source for the reduced
351 moment in the hybrid structure because the samples were
352 well protected with a thick bilayer of Al(7 nm)/
353 Al$_2$O$_3$(5 nm) over it (Fig. 4). The nuclear SLD of the CoO
354 layer adjacent to the Fe was found to be lower than the bulk
355 value ($\sim$4.27$\times$10^{-6} Å^{-2}) in the hybrid sample, suggesting a
356 reduced structural density of the upper layers rather than en-
357 hanced oxidation. Another possibility is that the reduced Fe
358 moment is a direct consequence of higher roughness of the
359 rubrene layer in hybrid structure. However, the PNR fitting
360 analysis showed that the roughness of the rubrene/Fe layer is
361 similar ($\sim$3 nm) in the two samples though there exists a
362 higher roughness at the top interface of the Fe layer in the
363 hybrid sample ($\sim$1.3 nm) compared to in rubrene sample (
364 $\sim$0.7 nm).
365   A more significant finding is that the nuclear SLD for Fe
366 is lower in the hybrid sample (Fig. 4) presumably indicating
367 that the structural density is reduced from that of bulk Fe. A
368 possible origin of this reduction emerges from an under-
369 standing of the growth of Fe at the first few layers, which can
370 be directly influenced by the structural properties of the un-
371 derlying rubrene layer. In the hybrid sample, the lower den-
372 sity of Fe follows from the lower packing density of the
373 underlying rubrene layer, which leads in turn to the higher

374 Fe/CoO interface roughness. Given the roughness of the
375 rubrene/Fe interface, the presence of subnanofilamentary
376 growth of Fe at this interface is probable in both samples.
377 Due to the lower packing density and the azimuthal growth
378 of rubrene molecules in hybrid structure, we can expect such
379 formations to be more common in these hybrid samples. The
380 structural properties of the top Fe electrode in hybrid
381 samples clearly affect its magnetic response and are respon-
382 sible for the reduced moment. Also, the higher interface
383 roughness of the top Fe layer in the hybrid structure will
384 have a direct influence on the exchange coupling and tend to
385 weaken the pinning of the Fe layer. Correspondingly, the
386 magnetic response of the Fe filaments at the Fe/Rubrene in-
387 terface may presumably differ from those in the center of the
388 layer. This will require a careful and systematic study that
389 will be followed in the future.

390 The weak exchange pinning of such formations at the
391 rubrene/Fe interface in HJ may lead to random spin fluctua-
392 tions that are detrimental for spin injection and transport. A
393 way to tailor this effect was to modify our junction stack. We
394 decided to exchange bias the bottom smooth Co layer and
395 made the top rough Fe layer free. MR measurements were
396 performed for the HJs with a rubrene thickness of 25 nm
397 (shown in Fig. 5). A MR of 7% was observed at 4.2 K,
398 reducing to ~4.5% at 77 K. No MR was noticed at room
399 temperature. A sharp switching between the parallel and the
400 antiparallel states are noted, suggesting the advantage of hav-
401 ing a strongly exchange pinned Co layer and a free top Fe
402 layer. The gradual decrease in MR with bias at 77 K (see Fig.
403 5 inset) indicated the good quality of the junctions. Further,
404 we were able to detect spin transport signals through thicker
405 rubrene films (~25 nm), hinting at a significant improve-
406 ment in our device performance. In comparison, no (or small
407 ~0.4% in some cases) MR was measured even in the most
408 stable thin rubrene barrier junctions (5 nm), confirming the
409 strong influence of interface ordering on spin injection.

410 In conclusion, we have observed the influence of the seed
411 layer on the growth morphology of the rubrene molecules at

FIG. 5. (Color online) MR measurement (minor loop) per-
formed on hybrid junction: $CoO(1)/Co(8)/Al_2O_3(0.6)/$
$Rub(25 \text{ nm})/Fe(12)$ at 77 and 4.2 K. The bottom Co electrode is
pinned to the CoO layer by cooling the sample in negative field.
Insets: top shows the increase in junction resistance with cool down
and the bottom shows the gradual decrease in MR with applied bias
at 77 K. The shift in the curve (toward left) is due to a residual
current from the power supply, flowing through the magnet.

412 the interface. Different growth mechanisms lead to a highly
413 anisotropic conduction mechanism that affects both charge
414 and spin injection and transport properties. Although this
415 study reveals better spin transport in molecularly ordered
416 films, PNR result shows a corresponding complex nature of
417 interface magnetic behavior, highlighting the open chal-
418 lenges that have to be carefully addressed and tailored if
419 organic materials are to reach their theoretical expectations
420 in spintronics application.

427 *vkarthik@mit.edu
428 [1] W. J. M. Naber, S. Faez, and W. G. van der Wiel, J. Phys. D **40**,
429 R205 (2007).
430 [2] Z. H. Xiong, Z. Di Wu, Valy Vardeny, and Jing Shi, Nature
431 (London) **427**, 821 (2004).
432 [3] T. S. Santos, J. S. Lee, P. Migdal, I. C. Lekshmi, B. Satpati, and
433 J. S. Moodera, Phys. Rev. Lett. **98**, 016601 (2007).
434 [4] V. Dediu, L. E. Hueso, I. Bergenti, A. Riminucci, F. Borgatti, P.
435 Graziosi, C. Newby, F. Casoli, M. P. De Jong, C. Taliani, and Y.
436 Zhan, Phys. Rev. B **78**, 115203 (2008).
437 [5] V. N. Prigodin, N. P. Raju, K. I. Pokhodnya, J. S. Miller, and A.
438 J. Epstein, Adv. Mater. **14**, 1230 (2002).
439 [6] Ö. Mermer, G. Veeraraghavan, T. L. Francis, Y. Sheng, D. T.
440 Nguyen, M. Wohlgenannt, A. Köhler, M. K. Al-Suti, and M. S.
441 Khan, Phys. Rev. B **72**, 205202 (2005).
442 [7] V. Coropceanu, J. Cornil, D. A. da Silvo Filho, Y. Olivier, R.
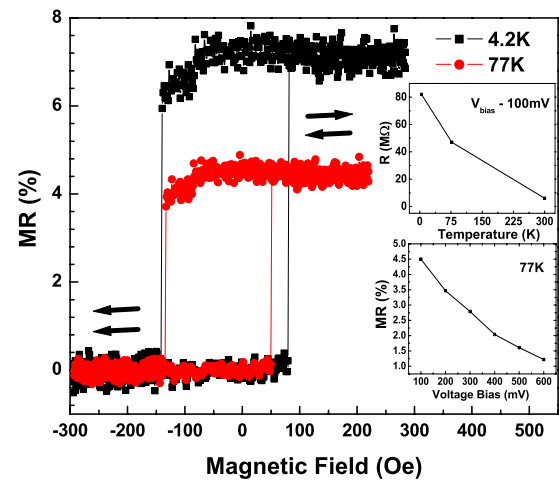443 Silbey, and J.-L. Bre'das, Chem. Rev. (Washington, D.C.) **107**,
444 926 (2007).
445 [8] M. A. Baldo and S. R. Forrest, Phys. Rev. B **64**, 085201 (2001).
446 [9] V. I. Arkhipov, E. V. Emelianova, Y. H. Tak, and H. Bässler, J.
447 Appl. Phys. **84**, 848 (1998).
448 [10] S. C. B. Mannsfeld, A. Virkar, C. Reese, M. F. Toney, and Z.
449 Bao, Adv. Mater. **21**, 2294 (2009).
450 [11] J. H. Shim, K. V. Raman, Y. J. Park, T. S. Santos, G. X. Miao, B.
451 Satpati, and J. S. Moodera, Phys. Rev. Lett. **100**, 226603 (2008).
452 [12] R. C. Jaklevic and J. Lambe, Phys. Rev. Lett. **17**, 1139 (1966); J.
453 Lambe and R. C. Jaklevic, Phys. Rev. **165**, 821 (1968).
454 [13] P. K. Hansma, *Tunneling Spectroscopy: Capabilities, Application
455 and New Techniques* (Plenum Press, New York, 1982).
456 [14] J. R. Weinberg-Wolf, L. E. McNeil, S. Liu, and C. Kloc, J. Phys.:
457 Condens. Matter **19**, 276204 (2007).
458 [15] A. L. Geiger, B. S. Chandrashekhar, and J. G. Adler, Phys. Rev.
459 **188**, 1130 (1969).
460 [16] D. C. Tsui, R. E. Dietz, and L. R. Walker, Phys. Rev. Lett. **27**,

1729 (1971).

[17] M. Wang, W. He, and T. P. Ma, Appl. Phys. Lett. **86**, 192113 (2005).

[18] S. Fratini, H. Xie, I. N. Hulea, S. Ciuchi, and A. F. Morpurgo, New J. Phys. **10**, 033031 (2008).

[19] http://www.physics.unc.edu/project/mcneil/MolecularAnimations/anim.php

[20] J. Kirtley, D. J. Scalapino, and P. K. Hansma, Phys. Rev. B **14**, 3177 (1976).

[21] N. M. D. Brown, R. B. Floyd, and D. G. Walmsley, J. Chem. Soc., Faraday Trans. 2 **75**, 17 (1979); N. M. D. Brown, W. J. Nelson, and D. G. Walmsley, *ibid.* **75**, 32 (1979).

[22] J. T. Hall and P. K. Hansma, Surf. Sci. **77**, 61 (1978).

[23] R. J. Kline, M. D. Mcgehee, and M. F. Toney, Nature Mater. **5**, 222 (2006).

[24] G. E. Thayer, J. T. Sadowski, F. Meyer zu Heringdorf, T. Sakurai, and R. M. Tromp, Phys. Rev. Lett. **95**, 256106 (2005).

[25] N. F. Mott, Philos. Mag. **19**, 835 (1969).

[26] G. P. Felcher, Phys. Rev. B **24**, 1595 (1981).

[27] M. R. Fitzsimmons and C. F. Majrkzak, *Modern Techniques for Characterizing Magnetic Materials* (Kluwer, Norwell, MA, 2005).

[28] K. V. O. Donovan and N. F. Berk, *Neutron Scattering from Magnetic Materials* (Elsevier, Amsterdam, The Netherlands).

[29] C. F. Majkrzak, Physica B **221**, 342 (1996).

[30] P. A. Kienzle, K. V. O'Donovan, J. F. Ankner, N. F. Berk, and C. F. Majkrzak, http://www.ncnr.nist.gov/reflpak (2000–2006).

[31] P. A. Kienzle, M. Doucet, D. J. McGillivray, K. V. O'Donovan, N. F. Berk, and C. F. Majkrzak, http://www.ncnr.nist.gov/reflpak (2000–2006).

AUTHOR QUERIES —

#1 AU: Please supply definition for "MTJ" if possible.

#2 AU: Although a caption makes reference to color online, Fig. 1 will appear black and white in print. Please make sure the caption makes sense to print reader.

#3 AU: Please check the supplied authors names for et al references.

#4 Au: Please verify that the first page should be '2294' not '1' in Ref. 10.

#5 Au: Please verify that the volume should be '77' not '76' in Ref. 22.

#6 Au: Please verify that the first page should be '1595' not 'R1595' in Ref. 26.